

# Multi-person Physics-based Pose Estimation for Combat Sports

Hossein Feiz<sup>1</sup> David Labb  <sup>1</sup> Thomas Romeas<sup>2</sup> Jocelyn Faubert<sup>2</sup> Sheldon Andrews<sup>1</sup>

<sup>1</sup>  cole de technologie sup  rieure, Montreal, Canada

{hossein.feizollah-zadeh-khoiee.1,david.labbe,sheldon.andrews}@etsmtl.ca

<sup>2</sup>Universit   de Montr  al, Montreal, Canada

{thomas.romeas,jocelyn.faubert}@umontreal.ca

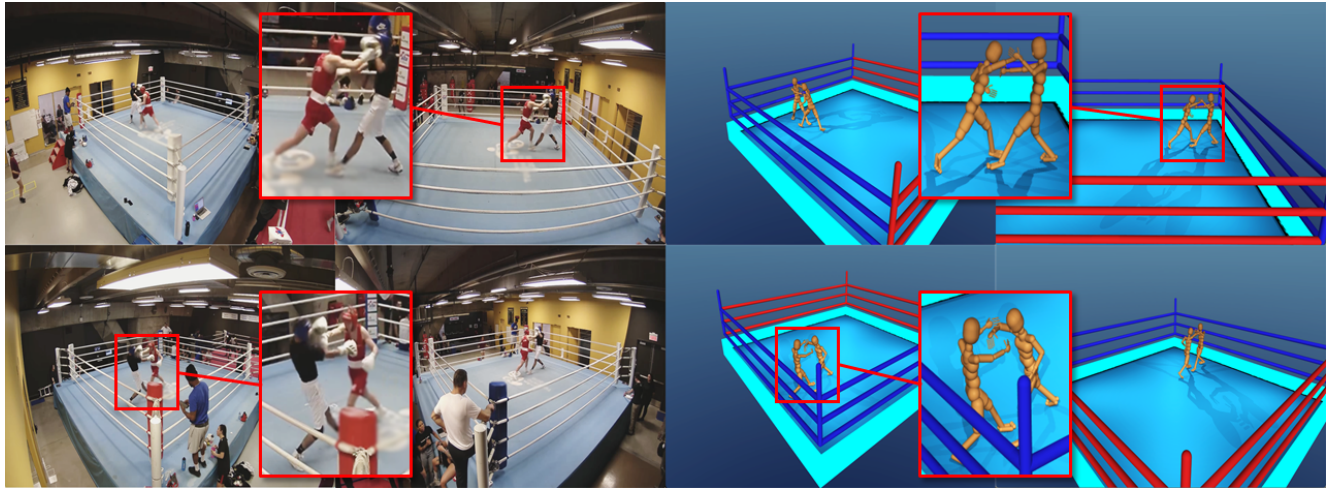


Figure 1. Multiple camera views of a boxing match (left) are processed by our pipeline to reconstruct the motion of multiple athletes inside a physics-based virtual environment (right).

## Abstract

We propose a novel framework for accurate 3D human pose estimation in combat sports using sparse multi-camera setups. Our method integrates robust multi-view 2D pose tracking via a transformer-based top-down approach, employing epipolar geometry constraints and long-term video object segmentation for consistent identity tracking across views. Initial 3D poses are obtained through weighted triangulation and spline smoothing, followed by kinematic optimization to refine pose accuracy. We further enhance pose realism and robustness by introducing a multi-person physics-based trajectory optimization step, effectively addressing challenges such as rapid motions, occlusions, and close interactions. Experimental results on diverse datasets, including a new benchmark of elite boxing footage, demonstrate state-of-the-art performance. Additionally, we release comprehensive annotated video datasets to advance future

research in multi-person pose estimation for combat sports. Results and dataset can be found on our [project page](#).

## 1. Introduction

Accurate 3D motion capture in combat sports remains a challenging problem due to rapid and complex athlete interactions, frequent occlusions, and crowded backgrounds. Traditional marker-based optical motion capture systems, while highly precise in controlled environments, become impractical in such dynamic contexts due to calibration issues and marker displacement caused by collisions. Inertial measurement unit (IMU)-based approaches provide freedom of movement but suffer from cumulative positional drift, especially in capturing precise spatial relationships between interacting athletes. Monocular vision-based systems eliminate tracking hardware constraints but typically lack precision and robustness, particularly under frequent occlusions.

and rapid motion conditions.

To address these challenges, we introduce a novel multi-stage, multi-view framework specifically tailored for combat sports scenarios such as boxing. Our approach effectively integrates robust multi-view 2D pose estimation, leveraging transformer-based architectures and epipolar geometry constraints, with weighted triangulation and spline smoothing for accurate initial 3D joint position estimates. A subsequent kinematic optimization refines these estimates, while our proposed multi-person physics-based trajectory optimization significantly enhances motion realism and resolves artifacts caused by inter-person penetrations and unrealistic interactions.

Experimental results demonstrate that our pipeline successfully reconstructs complex athlete interactions, faithfully adhering to physical constraints such as contact dynamics and collision avoidance. We evaluate our approach using comprehensive multi-view footage of elite boxers (illustrated in Figure 1) and further validate its accuracy using a supplementary dataset captured via synchronized optical motion capture systems. This supplementary dataset, along with detailed video annotations, will be publicly released to foster further research.

The contributions of our work can be summarized as follows:

- A robust multi-camera framework integrating kinematic and physics-based optimizations, enabling precise 3D pose estimation from sparse camera setups.
- A multi-person physics-based trajectory optimization method that significantly reduces inter-person penetration artifacts compared to existing state-of-the-art solutions.
- Two novel multi-view datasets: (i) Over 20 minutes of video footage featuring elite boxers during diverse, intense sparring scenarios, and (ii) sequences of human interactions accompanied by precise ground truth motions captured with an optical tracking system.

## 2. Related Work

### Multi-Person 3D Pose Estimation

Multi-person 3D human pose estimation has advanced significantly, transitioning from traditional two-stage pipelines [9] to unified, single-stage methods like ROMP [45] and Decoupled Regression [26], improving efficiency and robustness under occlusion. Transformer-based methods, such as POTR-3D [37], integrate temporal context and cross-person attention, smoothing predictions and resolving depth ambiguities. Weakly supervised approaches, like Ye et al. [59], reconstruct 3D motion from unlabeled web videos, leveraging self-supervised priors. Srivastav et al. [44] similarly introduced SelfPose3D, enabling accurate multi-view 3D estimation without requiring explicit 3D labels. Multi-view methods, like PlaneSweep-

Pose [32], directly fuse multiple views using plane-sweep stereo for efficient 3D estimation. Wang *et al.* [53] and Liao *et al.* [30] utilize transformers and geometric reasoning, significantly enhancing cross-view consistency. Zheng *et al.* [67] introduced PoseFormer, showing that transformers effectively capture temporal dependencies, inspiring subsequent multi-person approaches [37]. Diffusion models, like DiffPose [19] and Diff3DHPE [68], iteratively refine predictions, modeling ambiguity and ensuring reliable estimation under uncertainty.

### Multi-Person Physics-Based 3D Pose Estimation

Recent physics-based approaches to single- and multi-person 3D pose estimation integrate differentiable physics, biomechanics, and reinforcement learning to mitigate common artifacts such as foot sliding, body inter-penetration, and collisions [14, 17, 18, 21, 24, 41, 48, 50, 62, 65]. Differentiable physics-based methods explicitly enforce biomechanical constraints by jointly optimizing kinematic and dynamic parameters, ensuring physically realistic motion even under challenging athletic activities [17, 18, 41]. Similarly, reinforcement learning frameworks enable simulated agents to refine pose predictions through physics-informed rewards, reducing artifacts like floating body parts and penetration [21, 65]. Incorporation of physics modeling has further improved motion plausibility even when using sparse IMU signals as input, particularly by preventing foot sliding and stabilizing the motion [1, 48, 62]. Recent advances also address multi-person scenarios by enforcing mutual constraints, ensuring spatial coherence and collision-free motion [14, 50]. These methods often benefit from human-scene interaction cues, leveraging ground support and physical laws to promote robust pose estimation in dense crowds. Overall, the integration of physics-based modeling enhances realism and robustness across diverse applications, establishing a new standard for performance in both single- and multi-person pose reconstruction tasks. The incorporation of biomechanical constraints—as shown by Saleem et al.’s BioPose [42]—ensures realistic and immersive human motion. Moreover, reinforcement learning approaches, such as the imitation-based method proposed by Peng et al. [39], contribute to generating physically coherent human animations; collectively, these diverse methodologies offer robust and realistic multi-person motion estimation suitable for sports analysis, crowd dynamics [9, 28, 32, 40, 43].

### Multi-Person 3D Pose Estimation in Sports and VR Applications

Multi-person 3D pose estimation in sports poses significant challenges due to fast and unpredictable movements, frequent occlusions, and the need for fine-grained motion capture under high-intensity conditions [33]; early methods relied on controlled environments with multi-camera setups

or marker-based motion capture systems that, while accurate, proved costly and inflexible for real-world scenarios. Recent advances have shifted toward leveraging monocular or multi-view video feeds in unconstrained settings to enable applications such as player tracking, action recognition, and performance analysis in sports like basketball, soccer [25], and tennis [6, 51, 64]. To address issues arising from frequent occlusions and complex player interactions, many approaches now integrate spatio-temporal modules or graph-based methods to capture both short-term and long-term dynamics in high-speed sports sequences [55, 66], while Transformer-based architectures have shown promise in effectively modeling global context in dense player formations [16]. The emergence of large-scale sports datasets with rich annotations further facilitates improved generalization under domain-specific constraints [6, 29], spurring the development of specialized datasets and systems such as *SportsPose* [23], which features markerless motion capture of five high-speed sports validated against commercial marker-based systems, and *AthletePose3D* [61], which captures extreme dynamics across 12 sport motion types and approximately 1.3 million frames to achieve a reduction in pose error by nearly 69% (from 214 mm to 65 mm). For team sports, *WorldPose* [25] provides a large-scale multi-person dataset from the 2022 FIFA World Cup that captures 3D poses and trajectories of entire soccer teams using a static multi-camera setup, while tailored applications like *Reconstructing NBA Players* [69] demonstrate the integration of computer vision with domain-specific data to achieve high-resolution 3D mesh reconstruction from single broadcast images despite challenges such as complex poses, motion blur, and occlusions. In dense crowd scenarios, robust multi-view geometry frameworks that combine probabilistic reasoning and cross-view matching have proven effective [5]. In this work, we focus on using multi-person physics-based pose estimation of elite boxers captured during sparring sessions to robustly recover detailed 3D kinematics under challenging occlusion and rapid motion conditions. Our approach uniquely integrates physics simulation with advanced deep learning, enabling precise biomechanical analysis and offering new insights for performance optimization in competitive boxing.

### 3. Methodology

Figure 2 illustrates the overall architecture of our proposed framework, comprising four key stages: multi-view tracking, weighted triangulation, kinematic optimization, and dynamics-based trajectory refinement. Each stage is detailed in Sections 3.1 through 3.4.

#### 3.1. Multi-frame Multi-view Tracking IDs

Consistent tracking across multiple frames and views is crucial for accurate motion reconstruction, particularly when

camera setups are sparse. Limited overlapping fields of view and frequent occlusions pose significant challenges for reliably identifying and tracking the same individual across multiple camera views.

To achieve coherent tracking identities (**ids**), we utilize XMEm [8], a memory-based video segmentation method. This approach generates persistent identity labels within each single view, ensuring temporal consistency. Subsequently, we compute the centroids of the obtained bounding boxes (**bboxes**) and associate their assigned identities (**ids**) across multiple views, thus assigning unified identities for each individual in the scene.

To enhance cross-view matching reliability, we leverage epipolar constraints [7, 27]. These geometric constraints significantly narrow the matching search space by constraining centroid matching along epipolar lines defined by calibrated camera pairs, effectively reducing false associations.

We quantify cross-view consistency through epipolar distances as shown in Figure 3. Given the perspective projection matrix for camera  $j$  defined as

$$\mathbf{P}_j = \mathbf{K}_j [\mathbf{R}_j \mid \mathbf{t}_j],$$

where  $\mathbf{K}_j$  represents the intrinsic matrix,  $\mathbf{R}_j \in \mathbb{R}^{3 \times 3}$  denotes rotation, and  $\mathbf{t}_j \in \mathbb{R}^3$  denotes translation, we compute the fundamental matrix relating two camera views as

$$\mathbf{F}_{21} = \mathbf{K}_2^{-T} \mathbf{R} \mathbf{K}_1^T [\mathbf{K}_1 \mathbf{R} \mathbf{t}]_{\times},$$

where  $[\cdot]_{\times}$  indicates the skew-symmetric matrix operator.

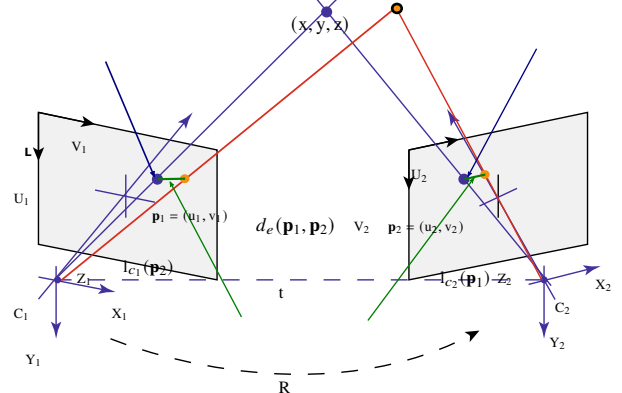


Figure 3. Illustration of the epipolar geometry distance for a pair of cross view 2D positions.

Given detected centroids  $\mathbf{p}_1$  in view 1 and  $\mathbf{p}_2$  in view 2, we define the epipolar distance [56] as

$$d_e(\mathbf{p}_1, \mathbf{p}_2) = d(\mathbf{p}_1, l_{c_1}) + d(\mathbf{p}_2, l_{c_2}), \quad (1)$$

where  $l_{c_1} = \mathbf{F}_{12} \mathbf{p}_1$  and  $l_{c_2} = \mathbf{F}_{21} \mathbf{p}_2$  represent the epipolar lines. The function  $d(\cdot, \cdot)$  calculates the perpendicular distance from a centroid to its corresponding epipolar line. By

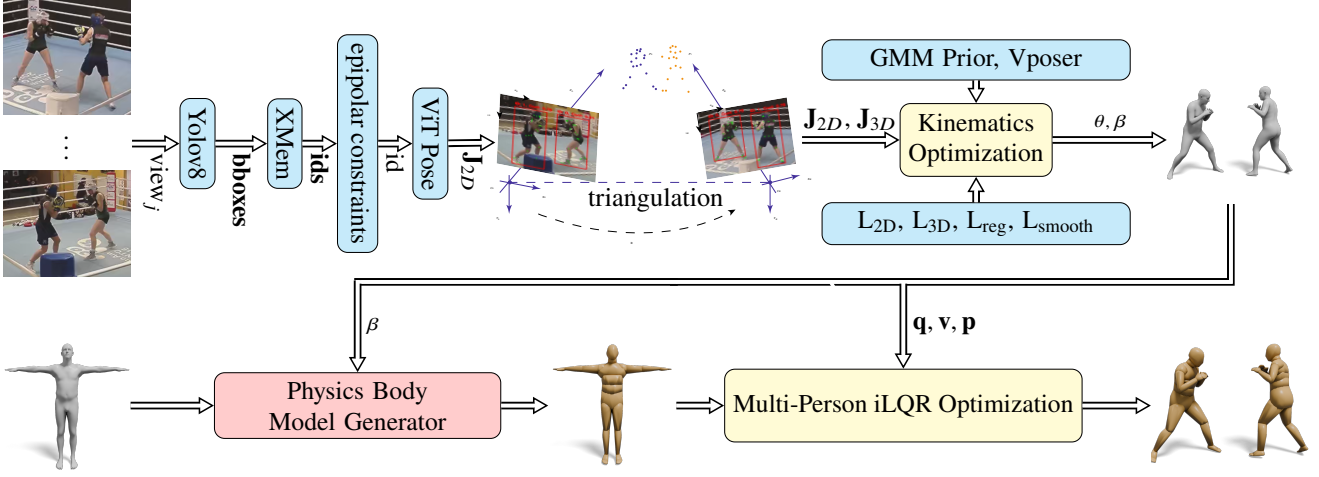


Figure 2. Overview of our proposed pipeline. Initially, bounding boxes (**bboxes**) and robust identity tracking (**id**) are generated for each individual in the scene. These tracking results facilitate accurate 2D pose estimation ( $\mathbf{J}_{2D}$ ) using ViTPose [57]. The subsequent triangulation process yields smoothed 3D keypoints ( $\mathbf{J}_{3D}$ ). These keypoints serve as input to the kinematic optimization stage, which outputs SMPL model parameters ( $\theta, \beta$ ). Finally, the optimized 3D joint positions ( $\mathbf{p}$ ), pose states ( $\mathbf{q}$ ), and velocity states ( $\mathbf{v}$ ), produced by our custom physics-based humanoid model generator, guide a model predictive controller employing the iLQR optimizer [20] to eliminate physical artifacts and refine motion quality.

minimizing  $d_e(\mathbf{p}_1, \mathbf{p}_2)$  across all camera pairs, we achieve consistent centroid associations and unified identity labels across multiple views and frames.

### 3.2. Weighted Triangulation and Filtering

We perform weighted triangulation to estimate the 3D positions of keypoints from their corresponding 2D detections across all  $N$  cameras. For each joint, we solve the following weighted linear system:

$$\begin{bmatrix} \mu_1(\mathbf{P}_{11} - \mathbf{u}_1\mathbf{P}_{31}) \\ \mu_1(\mathbf{P}_{21} - \mathbf{v}_1\mathbf{P}_{31}) \\ \vdots \\ \mu_N(\mathbf{P}_{1N} - \mathbf{u}_N\mathbf{P}_{3N}) \\ \mu_N(\mathbf{P}_{2N} - \mathbf{v}_N\mathbf{P}_{3N}) \end{bmatrix} \begin{bmatrix} x \\ y \\ z \\ 1 \end{bmatrix} = \begin{bmatrix} 0 \\ 0 \\ \vdots \\ 0 \end{bmatrix}, \quad (2)$$

where  $\mathbf{P}_{ij}$  denotes the  $i$ -th row of the projection matrix  $\mathbf{P}_j$  for camera  $j$ ,  $(\mathbf{u}_j, \mathbf{v}_j)$  represents the detected 2D joint coordinates, and  $\mu_j$  is the average detection confidence for camera  $j$ . Cameras providing higher-confidence detections thus have increased influence in the triangulation process. We solve Eq.2 efficiently using Singular Value Decomposition (SVD)[10].

To handle potential triangulation outliers and missing data, we interpolate and smooth each joint's trajectory using cubic spline interpolation. In scenarios where triangulation fails, we employ an extended Kalman filter (EKF) leveraging the joint's velocity, acceleration, and positional constraints to estimate stable and accurate 3D trajectories. This robust filtering ensures high-quality 3D reconstructions even from sparse and noisy multi-view detections.

### 3.3. Kinematics Optimization from Multi-View Keypoints

Our kinematics optimization leverages multi-view 2D keypoints ( $\mathbf{J}_{2D}$ ) and triangulated 3D keypoints ( $\mathbf{J}_{3D}$ ) to fit an SMPL model [34]. This fitting process minimizes discrepancies between the SMPL joints and observed keypoints, incorporating temporal smoothness and human motion priors to ensure natural and coherent motion trajectories.

The SMPL shape parameters ( $\beta \in \mathbb{R}^{10}$ ) for each individual are initialized from triangulated 3D keypoints, optimizing to minimize differences between predicted and observed limb lengths. Subsequently, pose parameters ( $\theta \in \mathbb{R}^{72}$ ) are estimated through optimization.

We formulate this optimization as the minimization of the following objective using the LBFGS optimizer [36] with history size 100, learning rate 1.0, and strong Wolfe conditions:

$$\begin{aligned} \min_{\theta} \quad & w_1 L_{2D} + w_2 L_{3D} + w_3 L_{reg} + w_4 L_{smooth} \\ & + w_5 L_{GMM} + w_6 L_{Vposer}. \end{aligned} \quad (3)$$

with weights  $w_1 = 0.001$ ,  $w_2 = 1.0$ ,  $w_3 = 0.01$ ,  $w_4 = 0.001$ ,  $w_5 = 0.0001$ ,  $w_6 = 0.0001$  determined empirically.

The **2D re-projection loss**  $L_{2D}$  aligns projected 3D joints with detected 2D keypoints [38]:

$$L_{2D} = \sum_{j \in \mathcal{V}} \sum_{i \in \mathbf{J}_{2D}} c_{j,i} \rho (\mathbf{J}_{proj_{j,i}} - \mathbf{J}_{2D_{j,i}}), \quad (4)$$

where  $c_{j,i}$  denotes confidence scores, we only consider 2D keypoints with confidence higher than 0.7, and  $\rho$  is the robust

Geman-McClure error function. The projection is given by  $J_{\text{proj}_{j,i}} = \mathbf{P}_j J_i(\theta, \beta)$ , where  $\mathbf{P}_j$  is the camera projection matrix, and  $\mathbf{P}_j$  and  $J(\theta, \beta) = \mathbf{W}\mathcal{M}(\theta, \beta)$  is the joint mapping from mesh vertices  $\mathcal{M}$  we only consider 2D keypoints.

The **3D alignment loss**  $L_{3D}$  ensures consistency with triangulated 3D keypoints:

$$L_{3D} = \sum_{i \in \mathbf{J}_{3D}} c_i \|J_i(\theta, \beta) - J_{3D,i}\|^2, \quad (5)$$

where  $J_{3D,i}$  is the triangulated joint  $i$  and  $c_i$  is the confidence of the 3D joint  $i$  which obtained from averaging the confidences of the 2D joints.

The **smoothness loss**  $L_{\text{smooth}}$  enforces temporal coherence by penalizing abrupt changes between consecutive frames:

$$L_{\text{smooth}} = \sum_t \|\theta^t - \theta^{t-1}\|^2 + \|\mathcal{M}(\theta^t, \beta) - \mathcal{M}(\theta^{t-1}, \beta)\|^2. \quad (6)$$

The regularization terms  $L_{\text{reg}}$ ,  $L_{\text{GMM}}$ , and  $L_{\text{Vposer}}$  further guide the optimization toward plausible human poses by penalizing unnatural or exaggerated configurations, significantly reducing jitter and noise.

Finally, the **prior loss** term penalizes unnatural poses of the SMPL skeleton. Specifically, we incorporate two priors into the loss function: the Gaussian Mixture Model (GMM) prior [4] and the Vposer prior [38]. These priors guide the optimization towards realistic human poses and reduce jittering artifacts. The losses are defined as:

$$L_{\text{GMM}} = \frac{1}{N} \sum_{i=1}^N \text{GMM}(\theta_i, \beta), \quad L_{\text{Vposer}} = \frac{1}{N} \sum_{i=1}^N (z(\theta_i))^2,$$

where the function  $z(\cdot)$  maps the full pose into a latent space defined by the Vposer prior.

### 3.4. Multi-person Dynamic Optimization

Although the kinematic optimization stage can estimate plausible full-body poses for multiple individuals, artifacts such as foot sliding, inter-body penetrations, and ground penetration can frequently occur. To address these physical implausibilities, we introduce a multi-person dynamics optimization stage. This stage employs individualized physics-based humanoid models, parameterized by the shape parameters ( $\beta$ ), significantly improving motion realism and robustness.

**Physics-based Humanoid.** To ensure the physics humanoid accurately reflects the joint positions estimated by the SMPL model, we implement a custom physics-based humanoid generator. This generator utilizes joint positions and SMPL mesh landmarks at a T-pose to create articulated rigid-body models with convex mesh-shaped collision geometries. Convex hull mesh dimensions are derived directly from SMPL mesh segmentation.



Figure 4. Illustration of SMPL to physics-based humanoid conversion for varying body shapes.

Our physics humanoid model contains 69 joint-angle degrees of freedom (DOFs) alongside a 6-DOF free root joint. The joints are primarily modeled as hinge joints, allowing realistic biomechanical articulation. The base skeleton of the humanoid follows the SMPL skeleton with an assigned average human body density of  $985 \text{ kg/m}^3$ .

Several examples of physics-based humanoid models generated using this approach are shown in Figure 4.

**Multi-humanoid Model.** We define the combined state of  $K$  physics-based humanoids at each timestep  $t$  as  $\mathbf{x}_t = (\mathbf{q}_t, \mathbf{v}_t)$ , where  $\mathbf{q}_t \in \mathbb{R}^{63K}$  and  $\mathbf{v}_t \in \mathbb{R}^{62K}$  represent the joint rotations and velocities, respectively. While  $\mathbf{q}_t$  uses minimal coordinate representation, we compute the 3D joint positions relative to each humanoid’s body reference frame, represented by  $\mathbf{p}_t \in \mathbb{R}^{21K}$ , to guide optimization. The root orientation is encoded as a quaternion. Additional details about the humanoid model are provided in the supplementary material.

**Dynamical Simulation.** Joint torques actuate our physics-based humanoid models, computed via a physics-informed version of the previous kinematic optimization. Unlike purely kinematic methods, our approach integrates biomechanical constraints and realistic contact interactions using an advanced physics simulator [47]. The humanoid’s state evolves according to:

$$\mathbf{x}_{t+1} \leftarrow f(\mathbf{x}_t, \mathbf{u}_t),$$

where  $\mathbf{u}_t \in \mathbb{R}^{56K}$  represents joint torques excluding direct root actuation.

**Trajectory Optimization.** Our trajectory optimization leverages iterative Linear Quadratic Regulation (iLQR) [20], minimizing the objective:

$$\min_{\mathbf{u}_{0:T}} \sum_{t=0}^T w_1 L_{\text{reg},t} + w_2 L_{p,t} + w_3 L_{v,t} + w_4 L_{\text{collision},t}, \quad (7)$$

with empirically determined weights  $w_1 = 0.001$ ,  $w_2 = 10$ ,  $w_3 = 0.1$ ,  $w_4 = 20$ . The terms  $L_{\text{reg}}$  includes  $\|\mathbf{v}_t\|^2$  and  $\|\mathbf{u}_t\|^2$  for minimizing velocity and control values which ensure smooth, realistic motion by penalizing deviations from reference positions and velocities, and excessive joint torques and velocities. The optimized trajectory is refined iteratively via feedback:

$$\Delta \mathbf{u}_t = \mathbf{K}_t \Delta \mathbf{x}_t + \alpha \mathbf{k}_t,$$

where the feedback gain  $\mathbf{K}_t$  and offset  $\mathbf{k}_t$  are updated at each iteration to achieve convergence. We employ a parallel line search for optimal step size  $\alpha$  within  $[\alpha_{\min}, 1]$ . Further details are provided in Tassa et al. [46].

To prevent persistent inter-penetrations from kinematic estimates, we add a collision penalty term in our trajectory optimization:

$$L_{\text{collision},t} = \sum_{(i,j) \in C_t} \phi(d_{\text{overlap}}(i, j)),$$

where  $C_t$  denotes colliding parts at time  $t$  with  $d_{\text{overlap}}(i, j)$  quantifying penetration depth and  $\phi$  growing rapidly (e.g., quadratically) with overlap; additionally, the physics engine enforces Coulomb friction and non-penetration via contact manifolds, ensuring physically compliant responses.

## 4. Experiments and Results

In this section, we report results from a series of experiments on two established multi-view benchmarks, *Campus* [15] and *Shelf* [3], as summarized in Table 4. We also evaluate our approach on two monocular datasets, *CHI3D* [13] and *Hi4D* [63], reported in Table 5. Three ablation studies demonstrate the role of physics constraints in our final results. Figure 5 shows example frames from various datasets.

**Supplementary Material.** Our supplementary video and additional documentation offer deeper insights into our approach. Notably, we present video clips of two boxers in practice, exemplifying the robustness of our pipeline in complex scenarios involving close interactions. We also include an ablation study on each subsystem of our pipeline, validating its design.

**Multi-view Benchmarks.** We first compare our method to state-of-the-art multi-view approaches on the *Campus* [15] (three cameras, three subjects) and *Shelf* [3] (five cameras, four subjects) datasets. Table 4 lists Percentage of Correctly estimated body Parts (PCP) [15], showing that on the *Shelf* dataset, our approach achieves the highest average PCP. On *Campus*, we are competitive with the best existing methods. For a detailed explanation of the metrics and additional ablations, see the supplementary material. As no dedicated multi-view physics-based approach is available for multi-person settings, we compare against existing multi-view and some monocular multi-person physics-based methods.

**Multi-Person Interaction Datasets.** To evaluate our method in comparison with the existing multi-person physics-based trackers, we apply our dynamics optimization using monocular footage. Keypoints and pose estimates are

extracted using SLAHMR [60], which is employed in Multiphys [50]. We utilized the same evaluation datasets as in [50]. These datasets exhibit significant inter-person interactions, where methods based solely on kinematics often struggle. We evaluated our method using two datasets with varying levels of interaction.

The CHI3D dataset [13] also includes some close interactions, and includes 127 motion sequences of five pairs of subjects performing everyday actions such as posing, pushing, and hugging. Each sequence is annotated with action labels and ground-truth 3D poses in the SMPL format, using four camera views. The Hi4D data set [63] involves more intense interactions, with 100 short motion sequences that contain close interactions and high contact ratios between subjects performing actions such as hugging, posing, dancing and playing sports. These sequences were captured with up to eight cameras and involve 20 unique pairs of participants. As shown in Table 5, our method outperforms existing methods in most physics-based metrics, except for penetration.

Table 1. Quantitative comparison on our supplementary dataset.

Method	$e_{\text{MPJPE}} \downarrow$	$e_{\text{foot},z} \downarrow$	$e_{\text{foot},v_{xy}} \downarrow$	$e_{\text{smooth}} \downarrow$
Kinematics	41.2	16.4	2.2	6.1
Dynamics	38.4	8.1	0.3	4.6

We also ablate the effect of single-person vs. multi-person physics optimization on CHI3D in Table 3. A single-person model cannot fully resolve interpersonal penetrations and yields larger pose errors. In contrast, our multi-person optimization significantly reduces these artifacts and improves accuracy. Detailed definitions of physics metrics appear in the supplementary material.

**Supplementary Dataset.** We also collected a custom two-person dataset with close interactions to evaluate foot-ground contacts and overall motion quality. Ground-truth trajectories come from a 24-camera OptiTrack system, and we capture RGB images from up to 4 cameras. The cameras were calibrated with OpenCV [54] and then aligned to the motion capture frame. Figure 5 shows some frames from this dataset.

Table 2 demonstrates our system’s robustness across different camera counts, retaining high PCP under fewer viewpoints. Although the final dynamics optimization can slightly reduce PCP due to the rigid-body model, Table 1 indicates that physics-based constraints improve the final motion quality by lowering foot sliding and jitter.

**Conclusion.** We introduced a new framework for creating multi-person physics-based animations from multi-view RGB video. Our pipeline comprises robust multi-person

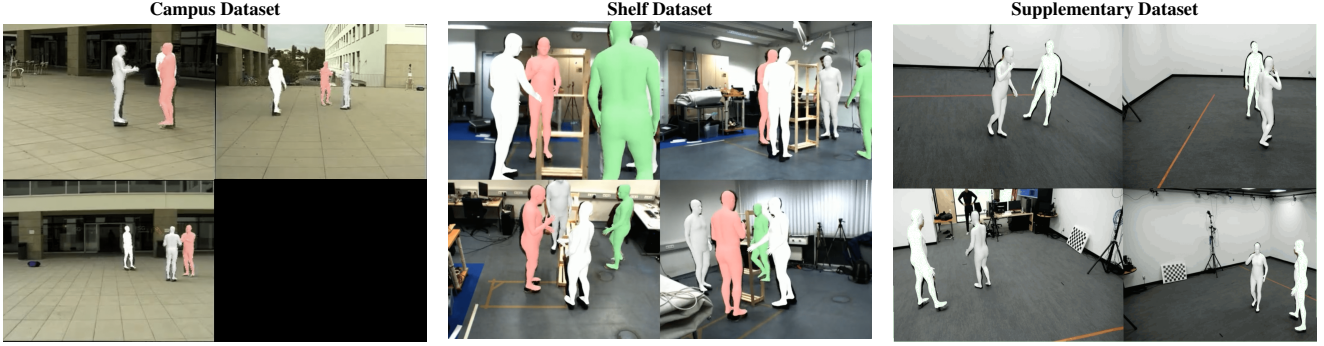


Figure 5. **Qualitative results** on various datasets. Our method accurately reconstructs human motion and outperforms or matches state-of-the-art kinematic methods.

Table 2. Comparison of PCP [%  $\uparrow$ ] on the supplementary dataset.

Method	4 cameras			3 cameras			2 cameras		
	Actor 1	Actor 2	Avg.	Actor 1	Actor 2	Avg.	Actor 1	Actor 2	Avg.
Triangulation	98.4	97.6	98.0	98.0	97.1	97.5	93.2	84.1	88.6
Kinematics	99.2	98.9	99.0	98.2	97.6	97.9	93.6	84.4	89.0
Dynamics	98.6	98.2	98.4	97.9	94.7	96.3	91.2	89.9	90.5

Table 4. Comparison of PCP [%  $\uparrow$ ] on the Campus and Shelf datasets.

Method	Campus				Shelf			
	Actor 1	Actor 2	Actor 3	Avg.	Actor 1	Actor 2	Actor 3	Avg.
Belagiannis et al. [2]	82.0	72.4	73.7	75.8	66.1	65.0	83.2	71.4
Belagiannis et al. [3]	93.5	75.7	84.4	84.5	75.3	69.7	87.6	77.5
Ershadi-Nasab et al. [12]	94.2	92.9	84.6	90.6	93.3	75.9	94.8	88.0
Dong et al. [11]	97.6	93.3	98.0	96.3	98.8	94.1	97.8	96.9
Huang et al. [22]	98.0	<b>94.8</b>	97.4	96.7	98.8	96.2	97.2	97.4
Tu et al. [49]	97.6	93.8	98.8	96.7	99.3	94.1	97.6	97.0
Lin and Lee [31]	98.4	93.7	<b>99.0</b>	97.0	99.3	96.5	98.0	97.9
Wang et al. [52]	99.3	95.1	97.8	97.4	98.2	94.1	97.4	96.6
Yang et al. [58]	98.2	94.6	98.2	97.0	99.5	96.0	97.7	97.7
ours (Triangulation)	<b>99.6</b>	92.2	97.6	96.5	<b>99.8</b>	95.4	<b>98.6</b>	<b>97.9</b>
ours (Kinematics)	98.5	93.5	94.4	95.5	<b>99.8</b>	<b>97.6</b>	<b>98.6</b>	<b>98.6</b>
ours (Dynamics)	98.1	93.6	94.2	95.3	98.9	<b>97.9</b>	98.2	98.3

Table 5. **Close interaction datasets.** Comparison on CHI3D [13] and Hi4D [63] with existing state-of-the-art trackers. Metrics: Penetration (Pen.), Ground Penetration (Gnd Pen.), Skating, Acceleration Error (Acc. Error), WA-MPJPE, W-MPJPE, and PA-MPJPE (joint) in mm.

Method	Pen.	Gnd Pen.	Skating	Acc. Error	WA-MPJPE	W-MPJPE	PA-MPJPE (joint)
SLAHMR [59]	139.3	4.4	<b>1.0</b>	<b>6.5</b>	100.9	177.1	83.5
EmbPose-MP [35]	40.2	2.6	2.8	7.7	126.7	214.7	96.5
MultiPhys [50]	<b>18.7</b>	3.2	2.7	7.4	98.1	174.7	80.4
Ours (Monocular)	21.4	<b>1.8</b>	2.3	6.7	<b>86.4</b>	<b>156.4</b>	<b>75.2</b>
SLAHMR [59]	367.3	12.2	4.9	<b>6.9</b>	<b>80.9</b>	121.6	<b>69.1</b>
EmbPose-MP [35]	<b>39.8</b>	3.8	<b>1.3</b>	12.7	115.3	148.8	92.9
MultiPhys [50]	51.1	2.4	3.5	9.6	84.8	<b>118.1</b>	71.2
Ours (Monocular)	67.2	<b>1.6</b>	1.9	8.3	91.1	124.1	82.1

tracking, triangulation, kinematics optimization, and a multi-person dynamics optimization. On multi-view benchmarks like Shelf [3], we achieve state-of-the-art performance, and our approach easily adapts to challenging real-world settings with minimal setup. By combining multi-view geometry with a physics layer, we resolve foot skating, body interpenetrations, and ground collisions. In the future, we will explore more efficient dynamics optimization strategies to further reduce runtime, aiming

Table 3. Comparing single-person vs. multi-person dynamics optimization on CHI3D [13].

Method	Pen.	WA-MPJPE	W-MPJPE	PA-MPJPE (joint)
Single-person Physics	114.9	117.3	174.5	92.1
Multi-person Physics	18.7	86.4	156.4	75.2

toward real-time deployment of the entire pipeline.

## References

- [1] Sheldon Andrews, Ivan Huerta, Taku Komura, Leonid Sigal, and Kenny Mitchell. Real-time physics-based motion capture with sparse sensors. In *Proceedings of the 13th European conference on visual media production (CVMP 2016)*, pages 1–10, 2016. 2
- [2] Vasileios Belagiannis, Sikandar Amin, Mykhaylo Andriluka, Bernt Schiele, Nassir Navab, and Slobodan Ilic. 3d pictorial structures for multiple human pose estimation. pages 1669–1676, 2014. 7
- [3] Vasileios Belagiannis, Sikandar Amin, Mykhaylo Andriluka, Bernt Schiele, Nassir Navab, and Slobodan Ilic. 3d pictorial structures revisited: Multiple human pose estimation. 38(10):1929–1942, 2016. 6, 7
- [4] Federica Bogo, Angjoo Kanazawa, Christoph Lassner, Peter Gehler, Javier Romero, and Michael J. Black. Keep it smpl: Automatic estimation of 3d human pose and shape from a single image. pages 561–578, 2016. 5
- [5] He Chen, Pengfei Guo, Pengfei Li, Gim Hee Lee, and Gregory Chirikjian. Multi-person 3d pose estimation in crowded scenes based on multi-view geometry. In *Computer Vision–ECCV 2020: 16th European Conference, Glasgow, UK, August 23–28, 2020, Proceedings, Part III 16*, pages 541–557. Springer, 2020. 3
- [6] Junwei Chen, Xinyu Liu, Roberto Garcia, and et al. Soccerpose: A benchmark for 3d multi-person pose estimation in soccer videos. In *CVPR*, 2023. 3
- [7] Long Chen, Haizhou Ai, Rui Chen, Zijie Zhuang, and Shuang Liu. Cross-view tracking for multi-human 3d pose estimation at over 100 fps. pages 3279–3288, 2020. 3
- [8] Ho Kei Cheng and Alexander G. Schwing. XMEm: Long-term video object segmentation with an atkinson-shiffrin memory model. 2022. 3
- [9] Yu Cheng, Bo Wang, Bo Yang, and Robby T. Tan. Monocular 3d multi-person pose estimation by integrating top-down and bottom-up networks. In *CVPR*, 2021. 2
- [10] Arcangelo Distante and Cosimo Distante. *Handbook of Image Processing and Computer Vision: Volume 3: From Pattern to Object*. Springer, 2020. 4
- [11] Junting Dong, Wen Jiang, Qixing Huang, Hujun Bao, and Xiaowei Zhou. Fast and robust multi-person 3d pose estimation from multiple views. pages 7784–7793, 2019. 7
- [12] Sara Ershadi-Nasab, Erfan Noury, Shohreh Kasaei, and Esmaeil Sanaei. Multiple human 3d pose estimation from multiview images. *Multimedia Tools Appl.*, 77(12):15573–15601, 2018. 7
- [13] Mihai Fieraru, Mihai Zanfir, Elisabeta Oneata, Alin-Ionut Popa, Vlad Olaru, and Cristian Sminchisescu. Three-dimensional reconstruction of human interactions. 2020. 6, 7
- [14] Mihai Fieraru, Mihai Zanfir, Teodor Szente, Eduard G. Bazavan, Vlad Olaru, and Cristian Sminchisescu. REMIPS: Physically consistent 3d reconstruction of multiple interacting people under weak supervision. In *Advances in Neural Information Processing Systems (NeurIPS)*, pages 16462–16473, 2021. 2
- [15] François Fleuret, Jerome Berclaz, Richard Lengagne, and Pascal Fua. Multicamera people tracking with a probabilistic occupancy map. 30(2):267–282, 2007. 6
- [16] Daisuke Fujii and Hideo Tanaka. Sportsformer: Transformer-based 3d human pose estimation for team sports. *arXiv preprint arXiv:2302.12345*, 2023. 3
- [17] Erik Gäßtner, Mykhaylo Andriluka, Hongyi Xu, and Cristian Sminchisescu. Trajectory optimization for physics-based reconstruction of 3d human pose from monocular video. In *Proceedings of the IEEE/CVF Conference on Computer Vision and Pattern Recognition (CVPR)*, pages 13071–13081, 2022. 2
- [18] Edgar Gäßtner, Davis Rempe, Siyu Tang, and Christian Theobalt. Differentiable physics-based human pose estimation. In *ECCV*, 2022. 2
- [19] Jia Gong, Lin Geng Foo, Zhipeng Fan, QiuHong Ke, Hossein Rahmani, and Jun Liu. Diffpose: Toward more reliable 3d pose estimation. In *CVPR*, 2023. 2
- [20] Taylor Howell, Nimrod Gileadi, Saran Tunyasuvunakool, Kevin Zakka, Tom Erez, and Yuval Tassa. Predictive Sampling: Real-time behaviour synthesis with MuJoCo. *arXiv preprint arXiv:2212.00541*, 2022. 4, 5
- [21] Buzhen Huang, Liang Pan, Yuan Yang, Jingyi Ju, and Yangang Wang. Neural mocon: Neural motion control for physically plausible human motion capture. In *Proceedings of the IEEE/CVF Conference on Computer Vision and Pattern Recognition (CVPR)*, pages 6407–6416, 2022. 2
- [22] Congzhentao Huang, Shuai Jiang, Yang Li, Ziyue Zhang, Jason Traish, Chen Deng, Sam Ferguson, and Richard Yi Da Xu. End-to-end dynamic matching network for multi-view multi-person 3d pose estimation. pages 477–493, 2020. 7
- [23] Christian Keilstrup Ingwersen, Christian Møller Mikkelstrup, Janus Nørtoft Jensen, Morten Rieger Hannemose, and Anders Bjorholm Dahl. Sportspose – a dynamic 3d sports pose dataset. In *Proceedings of the IEEE/CVF Conference on Computer Vision and Pattern Recognition Workshops (CVSports)*, 2023. 3
- [24] Mariko Isogawa, Ye Yuan, Matthew O’Toole, and Kris M. Kitani. Optical non-line-of-sight physics-based 3d human pose estimation. In *Proceedings of the IEEE/CVF Conference on Computer Vision and*

- Pattern Recognition (CVPR)*, pages 7013–7022, 2020. 2
- [25] Tianjian Jiang, Johsan Billingham, Sebastian Müksch, Juan Zarate, Nicolas Evans, Martin R Oswald, Marc Polleyfeys, Otmar Hilliges, Manuel Kaufmann, and Jie Song. Worldpose: A world cup dataset for global 3d human pose estimation. In *European Conference on Computer Vision*, pages 343–362. Springer, 2024. 3
- [26] Lei Jin, Chenyang Xu, Xiaojuan Wang, Yabo Xiao, Yandong Guo, Xuecheng Nie, and Jian Zhao. Single-stage is enough: Multi-person absolute 3d pose estimation. In *CVPR*, 2022. 2
- [27] Muhammed Kocabas, Salih Karagoz, and Emre Akbas. Self-supervised learning of 3d human pose using multi-view geometry. pages 1077–1086, 2019. 3
- [28] Jiefeng Li, Siyuan Bian, Chao Xu, Gang Liu, Gang Yu, and Cewu Lu. D&d: Learning human dynamics from dynamic camera. pages 479–496. Springer, 2022. 2
- [29] Yifan Li, Peng Zhou, and Chanwoo Park. Sportsdata: A large-scale dataset for sports pose estimation and action understanding. In *CVPR*, 2022. 3
- [30] Ziwei Liao, Jialiang Zhu, Chunyu Wang, Han Hu, and Steven L. Waslander. Multiple view geometry transformers for 3d human pose estimation. In *CVPR*, 2024. 2
- [31] Jiahao Lin and Gim Hee Lee. Multi-view multi-person 3d pose estimation with plane sweep stereo. pages 11886–11895, 2021. 7
- [32] Jiahao Lin and Gim Hee Lee. Multi-view multi-person 3d pose estimation with plane sweep stereo. In *CVPR*, 2021. 2
- [33] Han Liu, Adam Smith, and Michael Johnson. Marker-based and markerless techniques for sports motion analysis: A survey. In *ICCV Workshops*, 2013. 2
- [34] Matthew Loper, Naureen Mahmood, Javier Romero, Gerard Pons-Moll, and Michael J. Black. SMPL: A skinned multi-person linear model. *ACM Trans. Gr.*, 34(6):248:1–248:16, 2015. 4
- [35] Zhengyi Luo, Shun Iwase, Ye Yuan, and Kris Kitani. Embodied scene-aware human pose estimation. 2022. 7
- [36] Jorge Nocedal and Stephen J. Wright. *Numerical Optimization*. Springer, New York, NY, USA, 2 edition, 2006. 4
- [37] Sungchan Park, Eunyi You, Inhoe Lee, and Joonseok Lee. Towards robust and smooth 3d multi-person pose estimation from monocular videos in the wild. In *ICCV*, 2023. 2
- [38] Georgios Pavlakos, Vasileios Choutas, Nima Ghorbani, Timo Bolkart, Ahmed A. A. Osman, Dimitrios Tzionas, and Michael J. Black. Expressive body capture: 3d hands, face, and body from a single image. pages 10975–10985, 2019. 4, 5
- [39] Xue Bin Peng, Pieter Abbeel, Sergey Levine, and Michiel van de Panne. Deepmimic: Example-guided deep reinforcement learning of physics-based character skills. *ACM Trans. Gr.*, 37(4), 2018. 2
- [40] Davis Rempe, Tolga Birdal, Aaron Hertzmann, Jimei Yang, Srinath Sridhar, and Leonidas J. Guibas. Contact and human dynamics from monocular video. In *European Conference on Computer Vision (ECCV)*, 2020. 2
- [41] Davis Rempe, Leonidas J. Guibas, Aaron Hertzmann, Bryan Russell, Ruben Villegas, and Jimei Yang. Contact and human dynamics from monocular video. 2020. 2
- [42] Muhammad Usama Saleem, Gim Hee Lee, and Yujun Cai. Biopose: Biomechanically-accurate 3d pose estimation from monocular videos. *IEEE Transactions on Pattern Analysis and Machine Intelligence*, 2025. 2
- [43] Soshi Shimada, Vladislav Golyanik, Weipeng Xu, and Christian Theobalt. PhysCap. *ACM Trans. Gr.*, 39(6):1–16, 2020. 2
- [44] Vinkle Srivastav, Keqi Chen, and Nicolas Padoy. Selfpose3d: Self-supervised multi-person multi-view 3d pose estimation. In *CVPR*, 2024. 2
- [45] Yu Sun, Qian Bao, Wu Liu, Yili Fu, Michael J. Black, and Tao Mei. Monocular, one-stage, regression of multiple 3d people. In *ICCV*, 2021. 2
- [46] Yuval Tassa, Tom Erez, and Emanuel Todorov. Synthesis and stabilization of complex behaviors through online trajectory optimization. In *2012 IEEE/RSJ International Conference on Intelligent Robots and Systems*, pages 4906–4913, 2012. 6
- [47] Emanuel Todorov, Tom Erez, and Yuval Tassa. MuJoCo: A physics engine for model-based control. In *2012 IEEE/RSJ International Conference on Intelligent Robots and Systems*, pages 5026–5033. IEEE, 2012. 5
- [48] Shashank Tripathi, Lea Müller, Chun-Hao P. Huang, Omid Taheri, Michael J. Black, and Dimitrios Tzionas. 3d human pose estimation via intuitive physics. In *Proceedings of the IEEE/CVF Conference on Computer Vision and Pattern Recognition (CVPR)*, pages 4713–4725, 2023. 2
- [49] Hanyue Tu, Chunyu Wang, and Wenjun Zeng. Voxelpose: Towards multi-camera 3d human pose estimation in wild environment. pages 197–212, 2020. 7
- [50] Nicolas Ugrinovic, Boxiao Pan, Georgios Pavlakos, Despoina Paschalidou, Bokui Shen, Jordi Sanchez-Riera, Francesc Moreno-Noguer, and Leonidas Guibas. MultiPhys: Multi-person physics-aware 3d motion estimation. 2024. 2, 6, 7
- [51] Chao Wang, Lisa Huang, and Fan Zhang. Multi-athlete 3d pose estimation in challenging sports scenes. In *ECCV*, 2022. 3

- [52] Tao Wang, Jianfeng Zhang, Yujun Cai, Shuicheng Yan, and Jiashi Feng. Direct multi-view multi-person 3d pose estimation. pages 13153–13164, 2021. 7
- [53] Tao Wang, Jianfeng Zhang, Yujun Cai, Shuicheng Yan, and Jiashi Feng. Direct multi-view multi-person 3d pose estimation. In *NeurIPS*, 2021. 2
- [54] Y. M. Wang, Y. Li, and J. B. Zheng. A camera calibration technique based on opencv. In *The 3rd International Conference on Information Sciences and Interaction Sciences*, pages 403–406, 2010. 6
- [55] Xin Wei, Yin Zhao, and Han Liu. Volleygraph: Spatial-temporal graph convolution for volleyball pose estimation. In *WACV*, 2022. 3
- [56] Christian Wöhler. *3D computer vision: efficient methods and applications*. Springer Science & Business Media, 2009. 3
- [57] Yufei Xu, Jing Zhang, Qiming Zhang, and Dacheng Tao. ViTPose++: Vision transformer foundation model for generic body pose estimation. *arXiv preprint arXiv:2212.04246*, 2022. 4
- [58] Fan Yang, Shigeyuki Odashima, Sosuke Yamao, Hiroyuki Fujimoto, Shoichi Masui, and Shan Jiang. A unified multi-view multi-person tracking framework. *Computational Visual Media*, 10(1):137–160, 2024. 7
- [59] Vickie Ye, Georgios Pavlakos, Jitendra Malik, and Angjoo Kanazawa. Decoupling human and camera motion from videos in the wild. 2023. 2, 7
- [60] Vickie Ye, Georgios Pavlakos, Jitendra Malik, and Angjoo Kanazawa. Decoupling human and camera motion from videos in the wild. 2023. 6
- [61] Calvin C. K. Yeung, Tomohiro Suzuki, Ryota Tanaka, Zhuoer Yin, and Keisuke Fujii. AthletePose3D: A benchmark dataset for 3d human pose estimation and kinematic validation in athletic movements. *arXiv preprint arXiv:2503.07499*, 2025. 3
- [62] Xinyu Yi, Yuxiao Zhou, Marc Habermann, Soshi Shimada, Vladislav Golyanik, Christian Theobalt, and Feng Xu. Physical Inertial Poser (PIP): Physics-aware real-time human motion tracking from sparse inertial sensors. In *Proceedings of the IEEE/CVF Conference on Computer Vision and Pattern Recognition (CVPR)*, pages 13167–13178, 2022. 2
- [63] Yifei Yin, Chen Guo, Manuel Kaufmann, Juan Zarate, Jie Song, and Otmar Hilliges. Hi4D: 4d instance segmentation of close human interaction. 2023. 6, 7
- [64] Helen Yu, Rachel Duan, and Daehyeon Kang. Tennispose: Unconstrained multi-person 3d pose estimation for tennis video analysis. In *ACCV*, 2022. 3
- [65] Ye Yuan, Shih-En Wei, Tomas Simon, Kris Kitani, and Jason Saragih. SimPoE: Simulated character control for 3d human pose estimation. In *Proceedings of the IEEE/CVF Conference on Computer Vision and Pattern Recognition (CVPR)*, pages 7159–7169, 2021. 2
- [66] Qiang Zhang, Man Li, and Hao Wu. Sportsgcn: Multi-player pose tracking via graph convolution in sports videos. *IEEE TCSVT*, 2021. 3
- [67] Ce Zheng, Sijie Zhu, Matias Mendieta, Taojiannan Yang, Chen Chen, and Zhengming Ding. 3d human pose estimation with spatial and temporal transformers. In *ICCV*, 2021. 2
- [68] Jieming Zhou, Tong Zhang, Zeeshan Hayder, Lars Petersson, and Mehrtash Harandi. Diff3dhp: A diffusion model for 3d human pose estimation. In *ICCV Workshops*, 2023. 2
- [69] Luyang Zhu, Konstantinos Rematas, Brian Curless, Steven M. Seitz, and Ira Kemelmacher-Shlizerman. Reconstructing nba players. In *Proceedings of the European Conference on Computer Vision (ECCV)*, 2020. 3

## 5. Supplementary Materials

# Multi-person Physics-based Pose Estimation for Combat Sports

## Supplementary Material

### 5.1. Evaluation Metrics

We evaluate our approach using two main categories of metrics: **pose metrics** and **physics metrics**.

**Pose Metrics.** These measure pose accuracy and smoothness:

- **WA-MPJPE** (World-Aligned MPJPE). In some works, this refers to an MPJPE calculation where the predicted and ground-truth poses are aligned in the global (or “world”) coordinate system by a single rigid transformation (often estimated via a Procrustes-like method) *once* for the entire sequence. It does not allow a different transformation per frame.
- **W-MPJPE** (World PA First-MPJPE). This measures MPJPE after aligning *only the first frame* of the prediction and ground truth in the global coordinate system. The remaining frames are evaluated without further alignment, highlighting any drift that occurs over time.
- **PA-MPJPE** (Procrustes Aligned MPJPE). Each frame of the predicted pose is rigidly aligned to the corresponding ground-truth pose on a per-frame basis before computing MPJPE. This alignment factors out any frame-by-frame rigid transformations, emphasizing errors in limb positions or shape.
- **Acceleration Error (Acc. Error).** Evaluates discrepancies in acceleration between the predicted motion and ground truth, indicating whether the motion is jittery or overly smoothed.

**Physics Metrics.** These assess how physically plausible a motion sequence is:

- **Foot Skating (Skating).** Evaluates the extent to which feet slide on the ground when they should remain still.
- **Ground Penetration (Gnd Pen.).** Measures whether any body part intersects or penetrates the ground plane.
- **Inter-Person Penetration (Pen.).** Assesses collisions among different individuals by computing signed distance function (SDF) values. For each person, the SDF values from penetrating vertices of others are accumulated over all frames and averaged per person. This metric is measured in millimeters, whereas the other physics metrics are measured in meters.

Below are further details on the individual metrics:

#### 5.1.1. Percentage of Correct Parts (PCP)

The PCP metric quantifies the percentage of body parts whose endpoints are correctly localized. Let the ground-truth body part endpoints be  $\mathbf{s}_c$  and  $\mathbf{e}_c$ , and let  $\mathbf{s}_n$  and  $\mathbf{e}_n$  be their estimated counterparts. The part is considered correct if:

$$|\mathbf{s} - \mathbf{s}_c| + |\mathbf{e} - \mathbf{e}_c| \leq |\mathbf{s}_n - \mathbf{e}_n|. \quad (8)$$

#### 5.1.2. Mean Per Joint Position Error (MPJPE)

The MPJPE metric computes the mean Euclidean distance between predicted and ground-truth 3D joint positions:

$$\epsilon_{MPJPE} = \text{mean} \|\hat{\mathbf{p}}_t - \mathbf{p}_t^{GT}\|. \quad (9)$$

#### 5.1.3. Foot Floating and Sliding

**Foot Floating.** We compare the vertical position of the foot in the predicted motion to the ground truth:

$$\epsilon_{foot,z} = \text{mean} \|\hat{\mathbf{p}}_{foot,z} - \mathbf{p}_{foot,z}^{GT}\|. \quad (10)$$

**Foot Sliding.** We compare the foot’s horizontal velocity (on the XY plane) in the predicted motion to the ground truth:

$$\epsilon_{foot,v_{xy}} = \text{mean} \|\Delta \hat{\mathbf{p}}_{foot,v_{xy},t} - \Delta \mathbf{p}_{foot,v_{xy},t}^{GT}\|. \quad (11)$$

#### 5.1.4. Motion Smoothness

Smoothness is measured by (1) computing MPJPE on a 15-joint reduced skeleton plus the root, and (2) comparing keypoint velocities:

$$\hat{\mathbf{Jit}} = \|\hat{\mathbf{p}}_t - \hat{\mathbf{p}}_{t-1}\|, \quad (12)$$

$$\mathbf{Jit}^{GT} = \|\mathbf{p}_t^{GT} - \mathbf{p}_{t-1}^{GT}\|, \quad (13)$$

$$\epsilon_{smooth} = \text{mean} \|\mathbf{Jit}^{GT} - \hat{\mathbf{Jit}}\|. \quad (14)$$

### 5.2. Ablation Study

We conduct ablation experiments to illustrate the impact of key components in our framework.

**Number of Views.** Reducing camera views typically degrades 3D reconstruction due to weaker triangulation. Nevertheless, our method retains robustness in Table 6, even when views are sparse.

**Triangulation Filtering.** Spline smoothing and an Extended Kalman Filter (EKF) on keypoints significantly denoise the initial linear triangulation, improving subsequent kinematic optimization (Table 6).

**Prior (GMM + Vposer).** A Gaussian Mixture Model (GMM) prior in combination with Vposer narrows the pose parameter search space to more plausible solutions.

Table 6. Ablation Study on Shelf Dataset using PCP metric.

Method	Actor 1	Actor 2	Actor 3	Average
Baseline	99.8	97.6	98.6	98.6
Using 3 Views	98.3	98.1	98.6	98.3
Using 2 Views	97.6	48.1	96.4	80.7
No Filtering for Triangulation	99.8	94.9	97.9	97.5
No Prior	99.8	96.2	98.1	98.0
No 2D loss	91.6	76.2	81.2	83.0
No 3D loss	99.8	96.2	98.1	98.0
No pose regularization	99.8	95.7	98.5	98.0

Table 7. Configuration of the Humanoid used in physics optimization.

Joint	Force Range	Angle Range (rad)	Joint Type	No. Axes	Damping
Head	-40 to 40	-0.524 to 0.524	Hinge	3	20
Clavicle	-80 to 80	-0.349 to 0.349	Hinge	2	20
Femur	-300 to 300	-2.792 to 1.221	Hinge	3	20
Tibia	-160 to 160	0.01 to 2.967	Hinge	1	16
Foot	-120 to 120	-0.785 to 1.222	Hinge	2	12
Hand	-20 to 20	-1.57 to 1.57	Hinge	2	1
Humerus	-120 to 120	-1.571 to 1.571	Hinge	3	6
Lower Back	-300 to 300	-0.523 to 0.523	Hinge	3	24
Lower Neck	-120 to 120	-0.5236 to 0.5236	Hinge	3	40
Radius	-90 to 90	-2.967 to 0.174	Hinge	1	5
Toes	-20 to 20	1.570 to 0.349	Hinge	1	1
Wrist	-20 to 20	-3.14159 to 0	Hinge	1	1
Root	-	-	Free	-	-

**Regularization.** Pose regularization encourages smooth transitions between frames, reducing sudden jumps or unnatural artifacts.

### 5.3. CMU Humanoid Details

Table 7 shows the joint configurations for the CMU humanoid employed in physics optimization. Although the physics engine treats joints with three rotation axes as ball joints, we constrain these axes to mimic the behavior of *three consecutive hinge joints*, providing finer rotational control.

In summary, our pipeline combines noise-robust triangulation, strong pose priors, and physics-based optimization to yield smooth, physically plausible human motions under diverse scenarios, including sparse camera setups and noisy estimates.